International Journal of Control, Automation, and Systems 22(6) (2024) 1869-1882
http://dx.doi.org/10.1007/s12555-022-0643-1
ISSN:1598-6446 eISSN:2005-4092
http://www.springer.com/12555

Compensation-based Characteristic Modeling and Tracking Control for Electromechanical Servo Systems With Backlash and Torque Disturbance

Xiang Wang, Hanzhong Liu*, Jiali Ma, Yang Gao, and Yifei Wu

Abstract: For two-inertia servo mechanisms, the high order, backlash nonlinearity and external disturbance make the precise modeling and control difficult to implement. This article provides an easily implemented modeling and control strategy to deal with this problem. A characteristic modeling framework of disturbed nonlinear systems is proposed. To restrain the modeling error, the backlash nonlinearity and torque disturbance are observed by constructing a finite-time extended state observer (FESO) based on homogeneity properties and then the compensation action can be taken. Based on the compensated system, the discrete-time characteristic model is established using the sampled input-output data, which degrades the modeling complicacy. To estimate the model parameters, an adaptation law with projection algorithm is proposed using the tracking error and the estimation error as the excitation signal. A discrete-time second-order fast terminal sliding-mode control (DSFTSC) is proposed based on the characteristic model to stabilize the whole system, where an improved reaching law is designed to enhance the rapidity and weaken the chattering and the utilization of the fast terminal switching surface also speeds up the regression rate and decreases the tracking error. Finally, the effectiveness of the characteristic modeling, the adaptive law and the control scheme is validated by simulations in Matlab and experiments in a practical test rig, respectively.

Keywords: Backlash, characteristic model, servo mechanisms, sliding-mode control, torque disturbance.

1. INTRODUCTION

The growth of human society depends on the continuous progress of science and technology [1-4]. Motors have played important roles in modern industrial applications such as aerospace, marine, automobile, satellite antenna and semiconductor manufacturing [5-14]. In recent years, the development of economy and society brings increasing demands for high-performance controllers with high accuracy, fast response, good adaptability and anti-disturbance ability. However, the two-inertia servo mechanism is a high order, multivariable and strong coupling system, which complicates the control design process. Furthermore, the inner backlash nonlinearity and outer torque disturbance can highly affect the system performance and impose challenges to high-performance controller design. How to design a controller possessing good tracking behavior and practical implementability for actual digital servo system is a significant issue.

In recent researches, advanced control algorithms have been developed [15-26], e.g., adaptive control, sliding-mode control, active disturbance rejection control, and intelligent control. In adaptive control [15], update laws were designed based on the tracking error to estimate unknown parameters online, then a tracking controller was designed in the backstepping process to stabilize the sandwich-like system. Another adaptive control method [16] employed the filtered system dynamics to derive the estimation error, which achieved more accurate estimation of unknown parameters. Sliding-mode control (SMC) has been widely used with rapidity and robustness [17]. In global complementary SMC [18], an approach angle was inserted to the saturation function to regulate the boundary layer, which improved the global robustness to uncertainties and reduced oscillations. To simplify the design process, a practical fixed-time SMC with a high-gain compensator were designed [19], which could suppress the backlash nonlinearity and improve the convergence speed. The active disturbance rejection control in [20] designed a linear extended state observer (ESO) based on the nominal model to handle internal and external disturbances, then an internal model control scheme was combined with

Manuscript received July 6, 2022; revised July 17, 2023; accepted October 30, 2023. Recommended by Senior Editor Young IL Lee. This work was funded by the Major Project of Natural Science Research in Universities of Jiangsu Province (Grant No. 23KJA510003), the Six Talent Peaks Project in Jiangsu Province (Grant No. GDZB-027) and the NJIT Research Fund (Grant No. YKJ202110).

Xiang Wang and Hanzhong Liu are with the School of Automation, Nanjing Institute of Technology, No. 1, Hongjing Road, Jiangning District, Nanjing 211167, China, and Xiang Wang is also with the School of Automation, Nanjing University of Science and Technology, No. 200, Xiaolingwei Street, Xuanwu District, Nanjing 210094, China (e-mails: {wxnanjing, zdhxlhz}@126.com). Jiali Ma, Yang Gao, and Yifei Wu are with the School of Automation, Nanjing University of Science and Technology, No. 200, Xiaolingwei Street, Xuanwu District, Nanjing 210094, China (e-mails: ma920618@sina.com, gaoyangnjust@hotmail.com, wuyifei2017@126.com).
* Corresponding author.

the ESO to further improve the tracking performance. For high-order two-inertia systems, the backstepping technique is usually adopted for control design. A neural network state observer was designed to observe unknown system states in [21], then the backstepping technique is utilized to stabilize the whole system. The backstepping control was revised and a dynamic surface control was designed in [22], where differentiators were used to obtain the derivatives for virtual controllers. Compared to the dynamic surface control, the command filtered backstepping control was designed in [23] to further improve the tracking accuracy by adding a filtering error compensation system.

The backlash exists in the transmission part. When the speed direction of the driving part changes, the teeth of the driving gear leave the meshing surface and cross the backlash. At this time, the driven part is out of control. Then the driving gear remeshes with the driven gear and drive the driven part to rotate in reverse. In this process, the transmitted torque shows the deadzone and the system performance degrades or even becomes unstable due to the limit cycle or impact [27]. Since the backlash exists inside the system and the system order is relatively high, it is difficult to compensate the backlash directly. Therefore, the disturbance observer [28] or the intelligent approximator [29,30] was often used in the virtual controller, and the backlash was compensated in the backstepping process. Torque disturbance is another major factor related to the system performance, which can immediately affect the speed and then the position. Moreover, large torque disturbance even leads to instability. The torque disturbance in practical systems is difficult to measure, therefore sliding mode observers [31], disturbance observers [32] and ESOs [33,34] were often utilized.

For the two-inertia servo mechanism, most of the existing control strategies are designed using backstepping. Although many of them may have good performance, these control strategies are generally complicated due to the high order and complex structure of the traditional model. To deal with the backlash nonlinearity and external disturbance, neural networks, fuzzy logic systems or disturbance observers are employed in the backstepping process, which increases the complexity. Moreover, control algorithms designed with continuous time have to be discretized for application, which degrades the performance.

This motivates us to develop a discrete-time position tracking controller for practical systems. We aim to combine a new discrete characteristic modeling method with the discrete terminal sliding-mode control to facilitate the control system. Compared to the traditional modeling approach based on accurate dynamic analysis, the characteristic model is established as a low-order difference equation by making use of input and output data [35-37]. The parameters can be identified and the range can be determined with little prior knowledge. However, the online estimation of parameters is affected by the backlash effect and torque disturbance. To solve this problem, a finite-time ESO (FESO) is designed to observe the lumped disturbances for compensation in the inner loop. Then, based on the identified equation, a discrete-time second-order fast terminal sliding-mode controller (DSFTSC) is proposed to speed up the tracking rate and stabilize the whole system. The effectiveness of the characteristic modeling, the adaptive law and the control scheme is verified by simulations in Matlab and experiments in a practical servo system test rig, respectively. The contributions are as follows:

1) A characteristic modeling framework of disturbed servo mechanisms is proposed. Before the discrete-time modeling, the nonlinear part of backlash function and the torque disturbance are encapsulated into a lumped function. A FESO based on homogeneity properties is proposed to observe the lumped disturbance. Then, based on the compensated system, the characteristic model is established by input and output data. The modeling error caused by the disturbance is greatly weakened and the characteristic model output is equivalent to the original system output in steady state.
2) To obtain the values of model parameters, an adaptation law is proposed using the tracking error and the estimation error as the excitation signal. The parameter range can be determined and a projection algorithm is thus added to guarantee the estimation accuracy.
3) A DSFTSC is proposed based on the identified model. An improved reaching law is designed to enhance the rapidity and weaken oscillations. The fast terminal switching surface also speeds up the regression rate and decreases the tracking error.

2. SYSTEM DESCRIPTION

The electromechanical servo system illustrated in Fig. 1 is studied in this article. The motor is connected with the reducer and the small gear. The small gear engages with the gear ring, where the load is fixed. The servo motor can provide electromagnetic torque and power for the load through the transmission part. Since the current response is much faster than the speed response, the current dynamics can be ignored. The dynamics model is established as

$$\begin{cases} \dot{\theta}_d = \omega_d, \\ J_d\dot{\omega}_d + b_d\omega_d = n\tau_b - \tau_d, \\ \dot{\theta}_m = \omega_m, \\ J_m\dot{\omega}_m + b_m\omega_m = \tau_{em} - \tau_b, \\ \tau_{em} = c_t i_q, \end{cases} \tag{1}$$

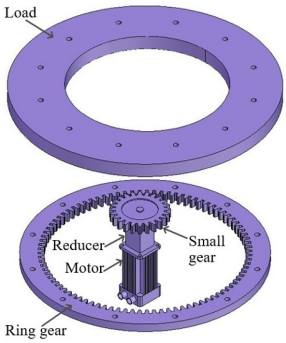

Fig. 1. Structural diagram of the electromechanical servo system.

where J_d, b_d, J_m, and b_m represent the load's and motor's inertia and friction factor, separately. θ_d, ω_d, θ_m, and ω_m represent the load's and motor's position and speed, separately. τ_{em}, τ_b, and τ_d represent the electromagnetic torque, elastic torque, and torque disturbance, separately. c_t represents the torque factor. i_q represents the q-axis current. n represents the reduction ratio. To describe the backlash, the elastic torque τ_b in (1) is depicted by the following differentiable dead-zone model [38].

$$\begin{cases} \tau_b = c_s \phi(\Delta\theta), \\ \phi(\Delta\theta) = \dfrac{1}{c_b} \ln\left[\dfrac{1+e^{c_b(\Delta\theta-\vartheta)}}{1+e^{-c_b(\Delta\theta+\vartheta)}}\right], \end{cases} \tag{2}$$

where $\Delta\theta = \theta_m - n\theta_d$ represents the relative position, 2ϑ represents the width of gear clearance at motor side. c_s and c_b represents the flexibility factor and approximation factor, respectively.

For this two-inertia servo system with backlash and torque disturbance, our task in this article is to design a digital position control algorithm for the practical system, such that the actual position follows the command signal with fast speed and high accuracy.

3. LUMPED DISTURBANCE ANALYSIS AND FESO DESIGN

For the purpose of application-oriented modeling, a characteristic model will be established and the parameters will be estimated online. However, the online estimation is affected by internal and external disturbances. Moreover, large disturbances may make the system unstable, which cannot satisfy the modeling conditions. To solve this problem, a characteristic modeling framework of disturbed servo mechanisms is proposed. The nonlinear part of backlash function and the torque disturbance are combined as a lumped function. A FESO based on homogeneity properties is proposed to observe the lumped function and then the appropriate compensation action can be taken.

3.1. Lumped disturbance analysis

Divide the elastic torque (2) into a linear part and a nonlinear part as

$$\tau_b = \tau_0 + \Delta\tau_b, \tag{3}$$

where $\tau_0 = c_s\Delta\theta$ and $\Delta\tau_b = \tau_b - \tau_0$. The nonlinear part of elastic torque $\Delta\tau_b$, together with the load-side and motor-side friction torque $b_d\omega_d$, $b_m\omega_m$ are regarded as the equivalent disturbance T_{eq}, which is converted to the system input side. Define the states and input as $x_1 = \theta_d$, $x_2 = \dot{x}_1$, $x_3 = \dot{x}_2$, $x_4 = \dot{x}_3$ and $u = i_q$, the system (1) can be transformed as follows:

$$\begin{cases} \dot{x}_1 = x_2, \\ \dot{x}_2 = x_3, \\ \dot{x}_3 = x_4, \\ \dot{x}_4 = bu - a_1 x_3 - a_2 T_{eq}, \end{cases} \tag{4}$$

where $b = c_t c_s n/J_m J_d$, $a_1 = -c_s(n^2 J_m + J_d)/J_m J_d$, $a_2 = c_t c_s n/J_m J_d$ and

$$\begin{aligned} T_{eq} = {} & \frac{1}{c_t} b_m \omega_m - \frac{J_m}{c_t c_s} \Delta\ddot{\tau}_b + \frac{J_m}{c_t c_s n}(b_d \ddot{\omega}_d + \dddot{\tau}_d) \\ & + \frac{1}{c_t n}(b_d \omega_d + \tau_d). \end{aligned} \tag{5}$$

Further considering the parametric uncertainties, we divide the system parameter in (4) as $b = b_0 + \Delta b$, where b_0 is the nominal part and Δb is the uncertain part. The lumped disturbance is defined as

$$f = \Delta b u - a_1 x_3 - a_2 T_{eq}. \tag{6}$$

Considering that the elastic torque model (2) is differentiable, and the other terms in the lumped disturbance is also differentiable, we make the following assumption.

Assumption 1: The lumped disturbance is differentiable and the derivative is bounded, i.e., $\dot{f} = \delta$, $|\delta| \le \bar{\delta}$.

3.2. FESO design and convergence proof

Definition 1 [39]**:** A function $V : \mathbb{R}^n \to \mathbb{R}$ is homogeneous of degree d for the positive weights $(r_1, \cdots, r_n)$, if $V(\lambda^{r_1}\varepsilon_1, \cdots, \lambda^{r_n}\varepsilon_n) = \lambda^d V(\varepsilon_1, \cdots, \varepsilon_n)$ for all $\lambda > 0$.

Definition 2 [39]**:** A vector field $\varphi : \mathbb{R}^n \to \mathbb{R}^n$ is homogeneous of degree d for the positive weights $(r_1, \cdots, r_n)$, if each component φ_i is a homogeneous function of degree $r_i + d$, i.e., $\varphi_i(\lambda^{r_1}\varepsilon_1, \cdots, \lambda^{r_n}\varepsilon_n) = \lambda^{r_i+d}\varphi_i(\varepsilon_1, \cdots, \varepsilon_n)$ for all $\lambda > 0$.

Lemma 1 [40]**:** If the continuous functions $V_1(x)$ and $V_2(x)$ are homogeneous of degree d_1 and d_2 for the weights $(r_1, \cdots, r_n)$, and $V_1(x)$ is positive definite, then the following inequality holds for every $x \in \mathbb{R}^n$.

$$\min_{\{z:V_1(z)=1\}}\{V_2(z)\} \cdot V_1^{\frac{d_2}{d_1}}(x) \le V_2(x) \le \max_{\{z:V_1(z)=1\}}\{V_2(z)\} \cdot V_1^{\frac{d_2}{d_1}}(x). \tag{7}$$

Lemma 2 [41]**:** For a system $\dot{x}(t) = f(x(t))$, if there exists a continuously differentiable and positive function $V(x)$, and some scalars $\lambda > 0$, $0 < \beta < 1$ such that $\dot{V}(x) \leq -\lambda V^{\beta}(x)$, then this system is finite-time stable.

Based on homogeneity properties, a FESO for the system (4) is constructed as

$$\begin{cases} \dot{z}_1 = z_2 - h_1 \mathrm{sig}^{\gamma_1}(z_1 - x_1), \\ \dot{z}_2 = z_3 - h_2 \mathrm{sig}^{\gamma_2}(z_1 - x_1), \\ \dot{z}_3 = z_4 - h_3 \mathrm{sig}^{\gamma_3}(z_1 - x_1), \\ \dot{z}_4 = z_5 + b_0 u - h_4 \mathrm{sig}^{\gamma_4}(z_1 - x_1), \\ \dot{z}_5 = -h_5 \mathrm{sig}^{\gamma_5}(z_1 - x_1), \end{cases} \tag{8}$$

where $\mathrm{sig}^{\gamma}(\cdot) = |\cdot|^{\gamma}\mathrm{sign}(\cdot)$, $z_1, \cdots, z_5$ are the estimation of $x_1, \cdots, x_4, f$, respectively. γ_i, $i = 1, \cdots, 5$, are the powers satisfying $\gamma_i = i\gamma - (i-1)$, $\gamma \in (4/5,\ 1)$. $h_i > 0$, $i = 1, \cdots, 5$, are the observer gains, which satisfy the following condition.

$$\begin{cases} h_1 h_2 - h_3 > 0, \\ h_3(h_1 h_2 - h_3) - h_1(h_1 h_4 - h_5) > 0, \\ h_3(h_1 h_2 - h_3)(h_1 h_4 - h_5) - h_5(h_1 h_2 - h_3)^2 \\ \quad - h_1(h_1 h_4 - h_5)^2 > 0. \end{cases} \tag{9}$$

Theorem 1: For the system (4) and Assumption 1, suppose that the FESO (8) is applied, then the observation errors converge into a bounded set within finite time.

Proof: Define the observation errors as $\xi_i = z_i - x_i$, $i = 1, \cdots, 4$, and $\xi_5 = z_5 - f$. Define an error vector as $\xi = [\xi_1, \cdots, \xi_5]^T$. Subtracting (4) from (8), we derive the observation errors dynamics as

$$\dot{\xi} = \varphi(\xi) - B\delta = \begin{bmatrix} \xi_2 - h_1 \mathrm{sig}^{\gamma_1}(\xi_1) \\ \xi_3 - h_2 \mathrm{sig}^{\gamma_2}(\xi_1) \\ \xi_4 - h_3 \mathrm{sig}^{\gamma_3}(\xi_1) \\ \xi_5 - h_4 \mathrm{sig}^{\gamma_4}(\xi_1) \\ -h_5 \mathrm{sig}^{\gamma_5}(\xi_1) \end{bmatrix} - B\delta, \tag{10}$$

where $\varphi(\xi)$ is a vector field, $B = [0,\ 0,\ 0,\ 0,\ 1]^{\mathrm{T}}$. In view of Definition 2, $\varphi(\xi)$ is homogeneous of degree $\gamma - 1$ with respect to the weights $(1, \gamma, 2\gamma - 1, 3\gamma - 2, 4\gamma - 3)$. Noting that the observer gains are limited as (9), we can construct a Hurwitz matrix as

$$A = \begin{bmatrix} -h_1 & 1 & 0 & 0 & 0 \\ -h_2 & 0 & 1 & 0 & 0 \\ -h_3 & 0 & 0 & 1 & 0 \\ -h_4 & 0 & 0 & 0 & 1 \\ -h_5 & 0 & 0 & 0 & 0 \end{bmatrix}, \tag{11}$$

and find two positive definite symmetric matrices P and Q making the equation $A^{\mathrm{T}}P + PA = -Q$ hold.

Firstly, we neglect δ in (10) and only consider the system $\dot{\xi} = \varphi(\xi)$. The Lyapunov function is constructed as

$$V(\xi) = \frac{1}{2}\chi^{\mathrm{T}} P \chi, \tag{12}$$

where

$$\chi = \left[\mathrm{sig}^{\frac{1}{\gamma_s}}(\xi_1),\ \mathrm{sig}^{\frac{1}{\gamma_s\gamma_1}}(\xi_2),\ \ldots,\ \mathrm{sig}^{\frac{1}{\gamma_s\gamma_4}}(\xi_5)\right]^{\mathrm{T}}, \tag{13}$$

and $\gamma_s = \prod_{i=1}^{5}\gamma_i$. Calculating the Lie derivative $L_{\varphi}V(\xi)$ of (12) along $\varphi(\xi)$ to obtain

$$L_{\varphi}V(\xi) = \left[\frac{\partial V}{\partial \xi_1}, \frac{\partial V}{\partial \xi_2}, \frac{\partial V}{\partial \xi_3}, \frac{\partial V}{\partial \xi_4}, \frac{\partial V}{\partial \xi_5}\right]\varphi(\xi). \tag{14}$$

One can verify by Definition 1 that $V(\xi)$ and $L_{\varphi}V(\xi)$ are homogeneous of degree $\alpha_1 = \frac{2}{\gamma_s}$ and $\alpha_2 = \frac{2}{\gamma_s} + \gamma - 1$ with respect to the weights $(1, \gamma, 2\gamma - 1, 3\gamma - 2, 4\gamma - 3)$, respectively. Then we can deduce from Lemma 1 that there exists a $\lambda_1 > 0$ which makes the following inequation hold.

$$L_{\varphi}V(\xi) \leq -\lambda_1 V^{\beta_1}(\xi), \tag{15}$$

where $\lambda_1 = -\max\limits_{\{z:V(z)=1\}}\{L_{\varphi}V(z)\}$ and $\beta_1 = \frac{\alpha_2}{\alpha_1} = 1 + \frac{(\gamma-1)\gamma_s}{2} < 1$.

Secondly, we consider δ in (4) and construct the Lyapunov function for the complete system (4) as

$$V_s(\xi) = \frac{1}{2}\chi^{\mathrm{T}} P \chi, \tag{16}$$

where χ and P are the same with those in (12). The derivative of (16) can be calculated as

$$\dot{V}_s(\xi) = L_{\varphi}V(\xi) - \chi^{\mathrm{T}} P \left[0, 0, 0, 0, \frac{1}{\gamma_s\gamma_4}|\xi_5|^{\frac{1}{\gamma_s\gamma_4}-1}\right]^{\mathrm{T}}\delta. \tag{17}$$

One can verify by Definition 1 that $V(\xi)$ and $\frac{\partial V_s(\xi)}{\partial \xi_5}$ are homogeneous of degree $\alpha_3 = \frac{2}{\gamma_s}$ and $\alpha_4 = \frac{2}{\gamma_s} - \gamma_4$ with respect to the weights $(1,\ \gamma,\ 2\gamma - 1,\ 3\gamma - 2,\ 4\gamma - 3)$. Then we can deduce from Lemma 1 that there exist λ_2 and λ_3 which make the following inequation hold.

$$\lambda_2 V_s^{\beta_2} \leq \frac{\partial V_s(\xi)}{\partial \xi_5} \leq \lambda_3 V_s^{\beta_2}, \tag{18}$$

where $\lambda_2 = \min\limits_{\{z:V_s(z)=1\}}\left\{\frac{\partial V_s(z)}{\partial z_5}\right\}$, $\lambda_3 = \max\limits_{\{z:V_s(z)=1\}}\left\{\frac{\partial V_s(z)}{\partial z_5}\right\}$, and $\beta_2 = \frac{\alpha_4}{\alpha_3} = 1 - \frac{\lambda_2\lambda_s}{2}$. Defining $\lambda_4 = \max\{|\lambda_2|, |\lambda_3|\}$, (17) can be deduced as

$$\begin{aligned} \dot{V}_s(\xi) &\leq -\lambda_1 V_s^{\beta_1} + \lambda_4\bar{\delta}V_s^{\beta_2} \\ &= -\lambda_1(1-\kappa)V_s^{\beta_1} - (\lambda_1\kappa V_s^{\beta_1-\beta_2} - \lambda_4\bar{\delta})V_s^{\beta_2}, \end{aligned} \tag{19}$$

where $0 < \kappa < 1$. Once $\lambda_1\kappa V_s^{\beta_1-\beta_2} \geq \lambda_4\bar{\delta}$, we have $\dot{V}_s(\xi) \leq -\lambda_1(1-\kappa)V_s^{\beta_1}$. It follows from Lemma 2 that $V_s \leq \left(\lambda_4\bar{\delta}/\lambda_1\kappa\right)^{\frac{1}{\beta_1-\beta_2}} \triangleq \bar{V}_s$ will be achieved in finite time

t_s, which satisfies $t_s \leq \frac{1}{\lambda_1(1-\beta_1)}(V_s(0))^{1-\beta_1}$. One can also derive that $\|\chi\| \leq \sqrt{\frac{2\bar{V}_s}{\lambda_{\min}(P)}} \triangleq \bar{\chi}$ and $|\xi_3| \leq \|\chi\|^{\gamma_3\gamma_4} \leq \bar{\chi}^{\gamma_3\gamma_4}$, which indicates the observation errors are bounded in finite time. It is noted that convergence is generally used for states, and stability is generally used for systems. Convergence emphasizes the property at terminal time, and stability emphasizes the non-divergence in entire process.

The observation z_5 of lumped disturbance f can be obtained by the FESO, then the compensator is designed as

$$u_c = -z_5/b_0. \tag{20}$$

Then, based on the compensated system, we will establish the characteristic model in the next section.

4. CHARACTERISTIC MODELING OF THE COMPENSATED SYSTEM

In traditional modeling approach, the accurate dynamic analysis is relatively difficult and the mathematical model has a complex form with many unknown parameters, which makes the control algorithm difficult to be implemented. Compared to the traditional approach, the characteristic model is established as a low-order difference equation. Only three model parameters need to be identified and the range can be determined with little prior knowledge. This approach provides a theoretical basis for discrete-time modeling of actual systems.

4.1. Introduction of modeling theory

A nonlinear system is given as

$$\dot{x}_1 = F(x_1, \cdots, x_N, u_1, \cdots, u_M), \tag{21}$$

where x_1 represents the system output, $x_i = x_1^{(i)}$, $i = 2, \cdots, N$, u_1 represents the system output, $u_j = u_1^{(j)}$, $j = 2, \cdots, M$.

Assumption 2 [36]**:** The properties of the system (21) are as follows:

1) Single input single output.
2) The power of u is 1.
3) If $x_i = 0$ and $u_j = 0$, then $F(\cdot) = 0$.
4) $F(\cdot)$ is differentiable and continuous for x_i and u_j, the partial derivatives are bounded.
5) $|F(x(t+T), u(t+T))| - |F(x(t), u(t))| < LT$, where $L > 0$ and T denotes the sampling period.
6) x_i and u_j are bounded in the practical system.

Lemma 3 [36]**:** For any nonlinear system that can be described as (21), if the conditions 1)-4) in Assumption 2 are satisfied, then the input-output dynamics of the system can be described by the following characteristic model

$$\begin{aligned} x(k+1) &= \rho_1(k)x(k) + \rho_2(k)x(k-1) + \sigma_0(k)u(k) \\ &\quad + \sigma_1(k)u(k-1) + \Delta(k), \end{aligned} \tag{22}$$

where $x(k) = x_1(k)$, $u(k) = u_1(k)$, $\rho_1(k)$, $\rho_2(k)$, and $\sigma_0(k)$ represent the model parameters and $\Delta(k)$ represents the modeling error. Furthermore, if the conditions 5 and 6 in Assumption 2 are also satisfied, then

1) The parameters are slow time-varying for a sufficiently small T.
2) The parameter range can be given before identification.
3) Using the same input signals, the practical system output can be approximated by the characteristic model output with a tolerable small error in dynamic process. In steady state, the two outputs are equivalent.

In practical application, only $\sigma_0(k)u(k)$ can be retained as the input item for simplicity.

4.2. Characteristic modeling and parameter adaption

For the position controller, the control object is composed of the servo system, compensator and speed controller. The system can be transformed into (21) by diffeomorphism. Then, the characteristic model is built based on Lemma 3 as

$$\begin{aligned} x(k+1) &= \rho_1(k)x(k) + \rho_2(k)x(k-1) + \sigma_0(k)u(k) \\ &\quad + \Delta(k) \\ &= \Phi^{\mathrm{T}}(k)\Theta(k) + \Delta(k), \end{aligned} \tag{23}$$

where $x(k) = \theta_d(k\Delta t)$ represents the model output, $u(k) = \omega_{md}(k\Delta t)$ represents the model input. $\rho_1(k)$, $\rho_2(k)$, and $\sigma_0(k)$ represent the parameters to be estimated and $\Delta(k)$ represents the modeling error. $\Phi(k) = [x(k),\ x(k-1),\ u(k)]^{\mathrm{T}}$ represents the data vector and $\Theta(k) = [\rho_1(k), \rho_2(k), \sigma_0(k)]^{\mathrm{T}}$ represents the parameter vector. According to [36], we give the parameter interval as $\rho_1 \in [2 - \varpi\Delta t - \varpi\Delta t^2 - o_1, 2 + \varpi\Delta t + \varpi\Delta t^2 + o_1]$, $\rho_2(k) \in [-1 - \varpi\Delta t - o_2, -1 + \varpi\Delta t + o_2]$, $\sigma_0(k) \in (0, \varpi\Delta t^2 + o_3]$, where o_1, o_2, and o_3 are small constants of the order $O(\Delta t^2)$.

Then we will design the parameter adaptation law. For convenience, let $\bullet_i$ represent the ith component of a vector $\bullet$, $\hat{\Theta}$ represent the estimate of Θ, and $\tilde{\Theta}$ represent the estimation error, i.e., $\tilde{\Theta} = \hat{\Theta} - \Theta$. The operation $\leq$ between two vectors is performed in terms of corresponding elements of vectors. A discontinuous projection is given as

$$\mathrm{Proj}_{\hat{\Theta}_i}(\bullet_i) = \begin{cases} 0, \text{ if } \hat{\Theta}_i = \hat{\Theta}_{i\max} \text{ and } \bullet_i > 0, \\ 0, \text{ if } \hat{\Theta}_i = \hat{\Theta}_{i\min} \text{ and } \bullet_i < 0, \\ \bullet_i, \text{ otherwise }, \end{cases} \tag{24}$$

where $i = 1, 2, 3$. Using both the model estimation error and the tracking error, an adaptation law for the model

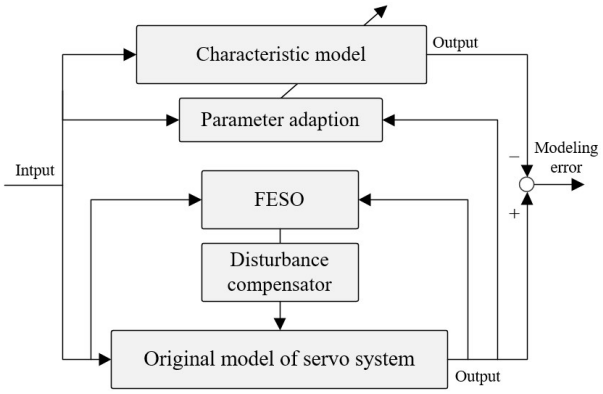

Fig. 2. Characteristic modeling of the compensated system.

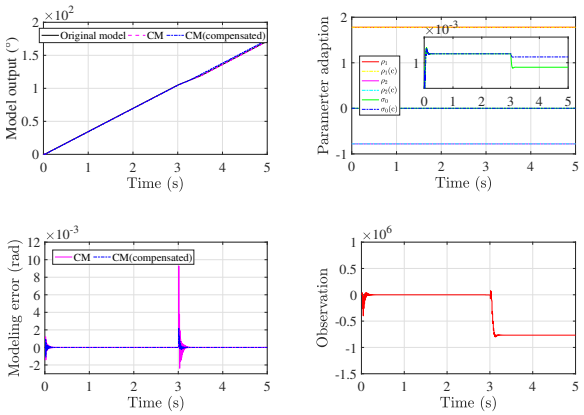

Fig. 3. Simulation results under step signal input.

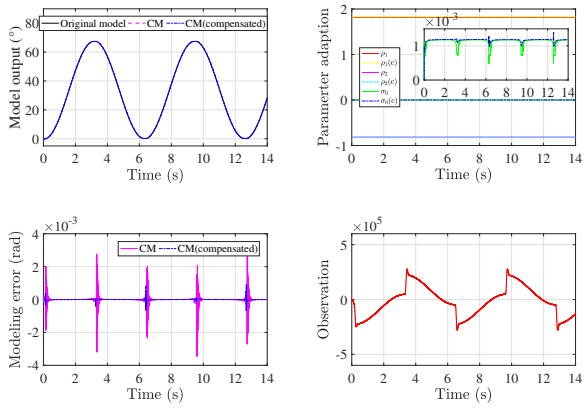

Fig. 4. Simulation results under sine signal input.

(23) is designed as

$$\begin{cases} \hat{\Theta}(k) = \hat{\Theta}(k-1) + \mathrm{Proj}_{\hat{\Theta}}(R(k)), \\ R(k) = \dfrac{[\Gamma_1 e_m(k) + \Gamma_2 \varsigma(k)]\,\Phi(k-1)}{\eta + \Phi^{\mathrm{T}}(k-1)\Phi(k-1)}, \end{cases} \tag{25}$$

where $\Gamma_1 > 0$, $\Gamma_2 > 0$, $\eta > 0$, $e_m(k) = x(k) - \hat{x}(k) - \iota \mathrm{sign}(x(k) - \hat{x}(k))$ represents the model estimation error, ι represents a small positive constant, $\hat{x}(k) = \Phi^{\mathrm{T}}(k-1)\hat{\Theta}(k-1)$, $\varsigma(k)$ represents the switching surface to be designed.

4.3. Simulation verification of characteristic model and disturbance compensator

In order to verify the FESO-based compensator and characteristic model, simulations are performed in Matlab. As shown in Fig. 2, the lumped disturbance including the backlash nonlinearity and torque disturbance are observed by the FESO and compensated by the compensator. Based on the compensated model, the parameters are estimated online. The modeling error represents the difference between the two outputs of original model and characteristic model. Then the characteristic models with and without FESO-based compensator are compared.

The parameters of the original model (1) are $J_d = 10.7$ kg·m^2, $J_m = 0.000323$ kg·m^2, $b_d = 0.00255$ N· m/kRPM, $b_m = 0.015$ N·m/kRPM, $R = 1.3\ \Omega$, $L = 37.5$ mH, $c_e = 67.2$ V/kRPM, $c_t = 1.11$ N·m/A, $c_s = 20$ N·m/rad, $n = 170$, $\vartheta = 0.005$ rad. The parameters of the adaptation law (25) are selected as $\eta = 0.95$, $\Gamma_1 = 0.6$, $\Gamma_2 = 0.3$. The parameters of the FESO (8) are selected as $h_1 = 2.5 \times 10^2$, $h_2 = 2.5 \times 10^4$, $h_3 = 1.25 \times 10^6$, $h_4 = 3.125 \times 10^7$, $h_5 = 3.125 \times 10^8$, $\gamma = 11/13$, $b_0 = 3 \times 10^5$. The simulation results are shown in Figs. 3 and 4.

In the first simulation, the input of original model is set as a 1000 RPM step signal and a 2.5 N·m torque disturbance is added after 3 s. We can see from the simulation results that the model outputs are slope position signals as shown in the "Model output" of Fig. 3, where CM represents the characteristic model. The parameter adaption are shown in Fig. 3, where ρ_1, ρ_2 and σ_0 represent the results without disturbance compensation and $\rho_1(c)$, $\rho_2(c)$ and $\sigma_0(c)$ represent the results with disturbance compensation. σ_0 is affected by the torque disturbance and falls a lot after 3 s, while $\sigma_0(c)$ generally keeps stable with the help of FESO-based compensator. The torque disturbance can be observed rapidly by the FESO as shown in the "Observation" of Fig. 3 and the influence can be much suppressed. The modeling error of CM jumps greatly at 3 s while the modeling error of compensated CM is much reduced as shown in the "Modeling error" of Fig. 3.

In the second simulation, the input of original model is set as a $1000\sin(t)$ RPM sine signal and the system is affected by the backlash nonlinearity. We can see from the simulation results that the model outputs are also sine position signals as shown in the "Model output" of Fig. 4. The parameter adaption of ρ_1, ρ_2, σ_0, $\rho_1(c)$, $\rho_2(c)$, and $\sigma_0(c)$ are shown in Fig. 4. σ_0 is affected by the backlash nonlinearity when the motor speed changes direction,

while the jumps in $\sigma_0(c)$ are greatly suppressed after disturbance compensation. The influence of backlash nonlinearity can be observed by the FESO as shown in the "Observation" of Fig. 4. Large periodic spikes appear in the modeling error of CM as shown in the "Modeling error" of Fig. 4 while these periodic spikes are much reduced in the modeling error of compensated CM.

Therefore, the output of the compensated characteristic model can accurately reproduce the output of original model. This verifies the equivalence between the characteristic model and original model.

5. CONTROLLER DESIGN AND STABILITY PROOF

In this section, the DSFTSC will be designed based on the characteristic model with estimated parameters to speeds up the regression rat and stabilize the system. The stability of the DSFTSC with parameter adaptation law will be analyzed.

5.1. DSFTSC design

Define the tracking error as

$$e(k) = x(k) - x_d(k), \tag{26}$$

where $x_d(k)$ represents the position command signal. Define the switching surface as

$$\varepsilon(k) = ce(k), \tag{27}$$

where $c > 0$ is a scale factor. Define the second-order switching surface as

$$\begin{aligned}\varsigma(k) &= \Delta\varepsilon(k) + p\varepsilon(k-1) \\ &\quad + q|\varepsilon(k-1)|^{\frac{\mu}{\nu}}\operatorname{sign}(\varepsilon(k-1)),\end{aligned} \tag{28}$$

where $\Delta\varepsilon(k) = \varepsilon(k) - \varepsilon(k-1)$, $0 < p < 1$, $q > 0$, and $0 < \frac{\mu}{\nu} < 1$. Design an improved reaching law for $\varsigma(k)$ as

$$\varsigma(k+1) = \varsigma(k) - m(k)\varsigma(k) - n(k)\operatorname{sign}(\varsigma(k)), \tag{29}$$

where $m(k) = \lambda_1 e^{-\kappa_1|\varsigma(k)|} + \lambda_0$, $n(k) = \lambda_2 e^{\kappa_2|\varsigma(k)|}$, λ_0, λ_1, λ_2, κ_1, and κ_2 are positive adjustable parameters.

The DSFTSC consists of two parts

$$u(k) = u_e(k) + u_s(k), \tag{30}$$

where the equivalent control law $u_e(k)$ is derived by solving $\varsigma(k+1) = 0$ as

$$\begin{aligned}u_e(k) = [c\hat{\sigma}_0(k)]^{-1}\big\{&c[x_d(k+1) - \hat{\rho}_1(k)x(k) \\ &- \hat{\rho}_2(k)x(k-1)] - (p-1)\varepsilon(k) \\ &- q|\varepsilon(k)|^{\frac{\mu}{\nu}}\operatorname{sign}(\varepsilon(k))\big\},\end{aligned} \tag{31}$$

and the switching control law $u_s(k)$ is derived based on the reaching law (29) as

$$\begin{aligned}u_s(k) = [c\hat{\sigma}_0(k)]^{-1}[&\varsigma(k) - m(k)\varsigma(k) \\ &- n(k)\operatorname{sign}(\varsigma(k))].\end{aligned} \tag{32}$$

Remark 1: In general non-adaptive approaches, the model parameters are selected as nominal values, which may be inaccurate. Comparatively, the parameters of DSFTSC are identified online, and the uncertainty can be weakened, which improves the performance. In general adaptive approaches, the update laws are designed to estimate unknown parameters, but the estimation accuracy cannot be guaranteed. Comparatively, the characteristic parameters have a small range, and the FESO is employed to reduce disturbances. Hence, the parameter adaptation in DSFTSC is easier and more accurate.

5.2. Stability proof

Lemma 4 [42] **:** Consider a scalar dynamical system

$$\begin{aligned}x(k+1) = x(k) - px(k) - q|x(k)|^{\frac{\mu}{\nu}}\operatorname{sign}(x(k)) \\ + \Lambda(k),\end{aligned} \tag{33}$$

where $0 < p < 1$, $q > 0$ and $0 < \mu/\nu < 1$. If $|\Lambda(k)| \le \bar{\Lambda}$ and $\bar{\Lambda} > 0$, then there is a finite number $k_x{}^*$, such that $\forall k \ge k_x{}^*$,

$$|x(k)| \le \psi(\mu/\nu)\cdot\max\left\{\left(\frac{\bar{\Lambda}}{q}\right)^{\frac{\nu}{\mu}}, \left(\frac{q}{1-p}\right)^{\frac{1}{1-\mu/\nu}}\right\}, \tag{34}$$

where $\psi(\mu/\nu) = 1 + (\mu/\nu)^{1/(\nu/\mu-1)} - (\mu/\nu)^{1/(1-\mu/\nu)}$.

Theorem 2: For the system (23), if the controller (30) and the adaptation law (25) are applied, then both the switching surface and the tracking error converge to bounded sets within finite steps.

Proof: By inserting the controller (30) back into the forward expression of (28), the dynamics of the switching surface can be written as

$$\begin{aligned}\varsigma(k+1) = \varsigma(k) - m(k)\varsigma(k) - n(k)\operatorname{sign}(\varsigma(k)) \\ - c\Phi^T(k)\tilde{\Theta}(k) + c\Delta(k).\end{aligned} \tag{35}$$

Construct a Lyapunov function as

$$V(k) = \frac{\Gamma_2\varsigma^2(k)}{\eta + \|\Phi(k-1)\|^2} + \left\|\tilde{\Theta}(k)\right\|^2. \tag{36}$$

In view of (25), the following deduction is held.

$$\begin{aligned}&\left\|\tilde{\Theta}(k)\right\|^2 \\ &\le \left\|\hat{\Theta}(k-1) + R(k) - \Theta(k)\right\|^2 \\ &\le \left\|\tilde{\Theta}(k-1)\right\|^2 + \frac{2\Gamma_1 e_m(k)\Phi^{\mathrm{T}}(k-1)\tilde{\Theta}(k-1)}{\eta + \|\Phi(k-1)\|^2} \\ &\quad + \frac{2\Gamma_2\varsigma(k)\Phi^{\mathrm{T}}(k-1)\tilde{\Theta}(k-1)}{\eta + \|\Phi(k-1)\|^2} \\ &\quad + \frac{{\Gamma_1}^2 e^2{}_m(k)\|\Phi(k-1)\|^2}{\left(\eta + \|\Phi(k-1)\|^2\right)^2}\end{aligned}$$

$$+\frac{\Gamma_2{}^2\varsigma^2(k)\|\Phi(k-1)\|^2}{\left(\eta+\|\Phi(k-1)\|^2\right)^2}+\frac{2\Gamma_1\Gamma_2 e_m(k)\varsigma(k)\|\Phi(k-1)\|^2}{\left(\eta+\|\Phi(k-1)\|^2\right)^2}. \tag{37}$$

Considering $2e_m(k)\varsigma(k) \le e_m{}^2(k)+\varsigma^2(k)$, (37) becomes

$$\begin{aligned}&\left\|\tilde{\Theta}(k)\right\|^2\\&\le\left\|\tilde{\Theta}(k-1)\right\|^2+\frac{2\Gamma_1 e_m(k)\Phi^{\mathrm{T}}(k-1)\tilde{\Theta}(k-1)}{\eta+\|\Phi(k-1)\|^2}\\&\quad+\frac{2\Gamma_2\varsigma(k)\Phi^{\mathrm{T}}(k-1)\tilde{\Theta}(k-1)}{\eta+\|\Phi(k-1)\|^2}\\&\quad+\frac{\left(\Gamma_1{}^2+\Gamma_1\Gamma_2\right)e^2{}_m(k)}{\eta+\|\Phi(k-1)\|^2}\\&\quad+\frac{\left(\Gamma_2{}^2+\Gamma_1\Gamma_2\right)\varsigma^2(k)}{\eta+\|\Phi(k-1)\|^2}.\end{aligned} \tag{38}$$

The first-order difference of $V(k)$ is calculated as

$$\begin{aligned}&\Delta V(k)\\&=V(k)-V(k-1)\\&=\frac{\Gamma_2\varsigma^2(k)}{\eta+\|\Phi(k-1)\|^2}-\frac{\Gamma_2\varsigma^2(k-1)}{\eta+\|\Phi(k-2)\|^2}\\&\quad+\frac{2\Gamma_1 e_m(k)\Phi^{\mathrm{T}}(k-1)\tilde{\Theta}(k-1)}{\eta+\|\Phi(k-1)\|^2}\\&\quad+\frac{2\Gamma_2\varsigma(k)\Phi^{\mathrm{T}}(k-1)\tilde{\Theta}(k-1)}{\eta+\|\Phi(k-1)\|^2}\\&\quad+\frac{\left(\Gamma_1{}^2+2\Gamma_1\Gamma_2\right)e^2{}_m(k)}{\eta+\|\Phi(k-1)\|^2}+\frac{\left(\Gamma_2{}^2+2\Gamma_1\Gamma_2\right)\varsigma^2(k)}{\eta+\|\Phi(k-1)\|^2}.\end{aligned} \tag{39}$$

Further considering $\Phi^{\mathrm{T}}(k-1)\tilde{\Theta}(k-1)= -e_m(k)-\iota\mathrm{sign}(x(k)-\hat{x}(k))+\Delta(k-1)$ and (35), we obtain

$$\begin{aligned}&\Delta V(k)\\&=V(k)-V(k-1)\\&=\frac{\Gamma_2\varsigma^2(k)}{\eta+\|\Phi(k-1)\|^2}-\frac{\Gamma_2\varsigma^2(k-1)}{\eta+\|\Phi(k-2)\|^2}\\&\quad+\frac{2\Gamma_1 e_m(k)[-e_m(k)-\iota\mathrm{sign}(x(k)-\hat{x}(k))+\Delta(k-1)]}{\eta+\|\Phi(k-1)\|^2}\\&\quad+\frac{2\Gamma_2 c^{-1}\varsigma(k)\begin{bmatrix}-\varsigma(k)+(1-m(k-1))\varsigma(k-1)\\-n(k-1)\mathrm{sign}(\varsigma(k))+c\Delta(k-1)\end{bmatrix}}{\eta+\|\Phi(k-1)\|^2}\\&\quad+\frac{\left(\Gamma_1{}^2+\Gamma_1\Gamma_2\right)e^2{}_m(k)}{\eta+\|\Phi(k-1)\|^2}+\frac{\left(\Gamma_2{}^2+\Gamma_1\Gamma_2\right)\varsigma^2(k)}{\eta+\|\Phi(k-1)\|^2}.\end{aligned} \tag{40}$$

By selecting the parameters as $\iota>\bar{\Delta}$, $\lambda_2>c\bar{\Delta}$ and considering $2\varsigma(k)\varsigma(k-1)\le\varsigma^2(k)+\varsigma^2(k-1)$, we can deduce (40) as

$$\begin{aligned}&\Delta V(k)\\&\le-\frac{\left(2\Gamma_1-\Gamma_1{}^2-\Gamma_1\Gamma_2\right)e_m{}^2(k)}{\eta+\|\Phi(k-1)\|^2}\\&\quad-\frac{\left[\Gamma_2 c^{-1}\left(1+m(k-1)\right)-\Gamma_2{}^2-\Gamma_1\Gamma_2-\Gamma_2\right]\varsigma^2(k)}{\eta+\|\Phi(k-1)\|^2}\\&\quad-\left[\frac{\Gamma_2}{\eta+\|\Phi(k-2)\|^2}-\frac{\Gamma_2 c^{-1}\left(1-m(k-1)\right)}{\eta+\|\Phi(k-1)\|^2}\right]\\&\quad\times\varsigma^2(k-1)\\&\triangleq-\upsilon_1 e_m{}^2(k)-\upsilon_2\varsigma^2(k)-\upsilon_3\varsigma^2(k-1).\end{aligned} \tag{41}$$

The parameters are selected to satisfy $\Gamma_1+\Gamma_2<2$, $c^{-1}(1+\lambda_0)>\Gamma_2+\Gamma_1+1$, $c^{-1}(1-\lambda_0)<\left(\eta+\|\Phi(k-1)\|^2\right)/\left(\eta+\|\Phi(k-2)\|^2\right)$. Then we have $\upsilon_1>0$, $\upsilon_2>0$, and $\upsilon_3>0$. By accumulating both sides from 1 to k, we obtain

$$\begin{aligned}&\sum_{i=1}^{k}\left[\upsilon_1 e_m{}^2(k)+\upsilon_2\varsigma^2(k)+\upsilon_3\varsigma^2(k-1)\right]\\&\le V(0)-V(k)\le V(0).\end{aligned} \tag{42}$$

Since $\upsilon_1 e_m{}^2(k)+\upsilon_2\varsigma^2(k)+\upsilon_3\varsigma^2(k-1)\ge 0$ and $\|\Phi(k)\|$ is bounded, we can derive that $\lim_{k\to\infty}|e_m(k)|=0$ and $\lim_{k\to\infty}|\varsigma(k)|=0$, that is, for any $\varpi_\varsigma>0$, there exists a $k_\varsigma{}^*\ge 0$ such that $|\varsigma(k)|<\varpi_\varsigma$, $\forall k\ge k_\varsigma{}^*$. Rewrite (28) to obtain the dynamics of switching surface

$$\begin{aligned}\varepsilon(k)&=\varepsilon(k-1)-p\varepsilon(k-1)\\&\quad-q|\varepsilon(k-1)|^{\frac{\mu}{\nu}}\mathrm{sign}(\varepsilon(k-1))+\varsigma(k).\end{aligned} \tag{43}$$

In view of Lemma 4, we can draw the conclusion that there exists $\varpi_\varepsilon>0$ and $k_\varepsilon{}^*\ge 0$ such that $|\varepsilon(k)|<\varpi_\varepsilon$, $\forall k\ge k_\varepsilon{}^*$, which indicates the switching surface and tracking error converge into bounded sets in finite steps.

Remark 2: In Theorem 1, the Lyapunov function is chosen as the general form, and the finite-time boundedness of the estimation error is proved. However, the asymptotic convergence of the estimation error has not been given, which needs to be further studied. In Theorem 2, the switching surface and the estimation error vector are both included in the Lyapunov function, and the stability of the closed-loop system is proved. However, there is no separate proof of the convergence of parameter estimation error, which remains a challenge.

Remark 3: Compared to most existing control strategies for two-inertia servo systems using the backstepping methods, this paper propose a practical discrete-time control design method. To reduce the influence of the backlash nonlinearity and the torque disturbance, a FESO

based on homogeneity properties is designed in the inner loop. Then, a characteristic model is built for the compensated system with a simplified form. Finally, a DSFTSC is proposed, where the system parameters are updated by the adaptation law and the fast terminal switching surface speeds up the convergence rate. The proposed controller can be directly implemented in practical systems without discretization.

6. EXPERIMENTAL VALIDATION

6.1. Test rig and parameter adjustment

The test rig of the servo turntable is shown in Fig. 5, which consists of the motor drive, the power box, the mechanical framework, the permanent magnet synchronous motor, the reducer, the gears and the load. The control diagram is given in Fig. 6. The command is set in the upper computer, and the information can be transmitted between the upper computer and motor drives via the controller area network (CAN) bus. The digital signal processor (DSP) and complex programmable logic device (CPLD) are utilized in the motor drive for system control and circuit protection, respectively. The power box provide high and low-voltage power for the motor drive. The intelligent power module (IPM) inverts direct current into three-phase alternating current with variable amplitude and frequency. The position and current are measured by the resolver and the Hall current sensor, respectively. The motor drive runs control algorithms and generates power drive signals for the motor. The system parameters are given in Table 1.

For comparative studies, the dynamic surface control (DSC), the DSFTSC without FESO are selected to compare with the proposed DSFTSC+FESO. The DSC can be designed with reference to the idea in [43] as follows: The tracking errors are defined as $e_1 = x_1 - x_d$, $e_2 = x_2 - \alpha_1$, $e_3 = x_3 - \alpha_2$, and $e_4 = x_4 - \alpha_3$. The virtual controllers are designed as $\alpha_1 = -k_1 e_1 + \dot{x}_d$, $\alpha_2 = -k_2 e_2 - e_1 + \dot{\alpha}_1$ and $\alpha_3 = -k_3 e_3 - e_2 + \dot{\alpha}_2$, and the derivative of α_i is obtained by the differentiator in [43]. The actual controller is $u = b^{-1}[-k_4 e_4 - e_3 + \dot{\alpha}_3 + a_1 x_3 + a_2 T_{eq}]$, where $k_i > 0$ is the control gain.

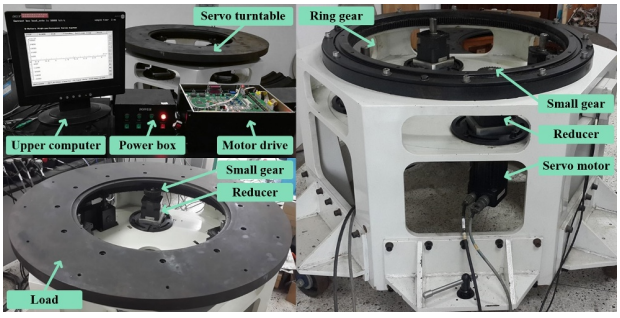

Fig. 5. Test rig of the electromechanical servo system.

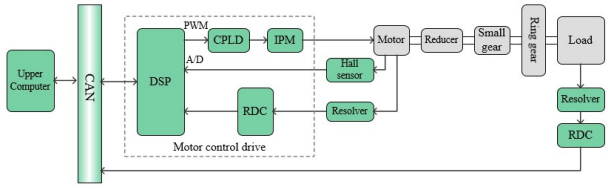

Fig. 6. Control system diagram of the electromechanical servo system.

Table 1. System parameters of the test-rig.

Component	Parameter	Value
Motor	Rated speed	3000 RPM
	Rated torque	7.4 N·m
	Torque coefficient	1.11 N·m/A
	Rated power	2.2 kW
	Viscous friction	0.015 N·m/kRPM
	Inertia	0.000323 kg·m^2
Reducer	Rated speed	4000 RPM
	Rated ratio	20
	Inertia	0.000141 kg·m^2
Load	Mass	275 kg
	Inertia	10.7 kg·m^2

After the tuning process, the parameters of DSC are selected as $k_1 = 60$, $k_2 = 100$, $k_3 = 15$, and $k_4 = 30$. The parameters of DSFTSC (30) are selected as $c = 0.8$, $\iota = 0.005$, $\mu/\nu = 9/11$, $p = 0.9$, $q = 0.45$, $\lambda_0 = 0.4$, $\lambda_1 = 0.2$, $\lambda_2 = 0.005$, $\kappa_1 = 0.1$, $\kappa_2 = 0.015$. The parameters of adaptation law (25) are selected as $\eta = 0.95$, $\Gamma_1 = 0.2, \Gamma_2 = 0.05$. In DSFTSC+FESO, an extra FESO is added and the parameters of FESO (8) are selected as $b_0 = 1.15 \times 10^6$, $\gamma = 13/15$, $h_1 = 7.5 \times 10^1$, $h_2 = 2.25 \times 10^3$, $h_3 = 3.38 \times 10^4$, $h_4 = 2.53 \times 10^5$, $h_5 = 7.59 \times 10^5$.

6.2. Experimental results and analysis

6.2.1 Sine wave tracking

The reference position signal is set as $\pi/3 \cdot [\sin(t - \pi/2) + 1]$ and the experimental results of three control algorithms are given in Fig. 7 and Table 2, where RMSE represents the root mean squared error and MAE represents the maximum absolute error. When tracking sine waves, the control algorithms generate position errors with periodic spikes. These periodic spikes are caused by the backlash nonlinearity when the motor changes direction. The DSC cannot well suppress the backlash influence and shows the largest position error. On the one hand, the model parameters in DSC are selected as the nominal values, which may be inaccurate, resulting in lower control performance. On the other hand, compared to the power terms in DSFTSC, only linear terms of errors are employed in DSC, leading to larger error. The DSFTSC generates smaller position error than DSC. This is because the model parameters in DSFTSC are adapted online, and

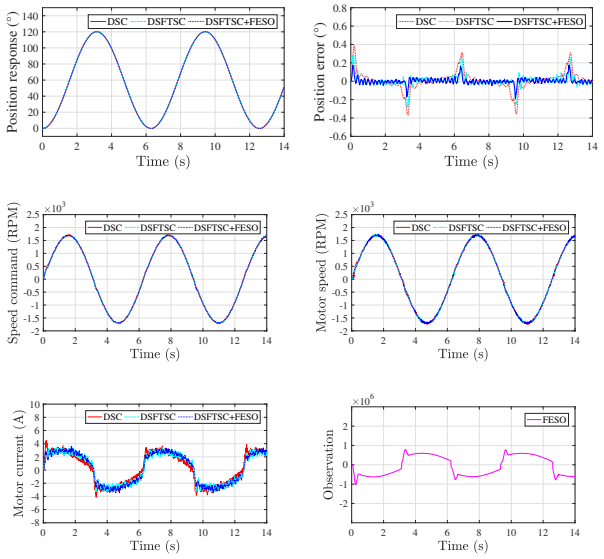

Fig. 7. Experimental results of sine wave tracking.

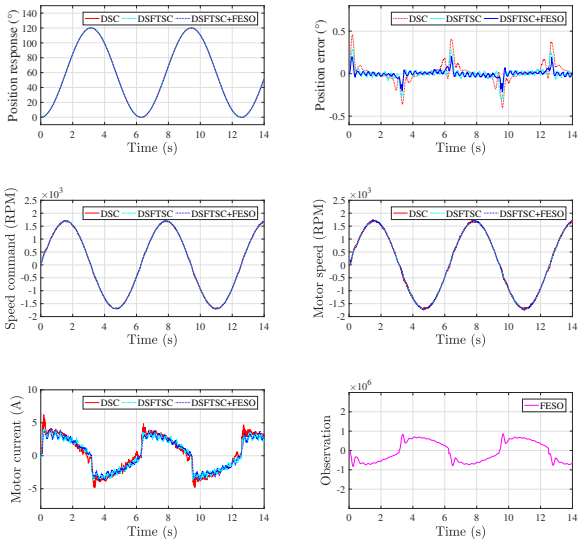

Fig. 8. Experimental results of sine wave tracking with increased inertia.

Table 2. Performance indices of sine wave tracking.

	RMSE	MAE
DSC	0.0966	0.385
DSFTSC	0.0553	0.285
DSFTSC+FESO	0.0336	0.189

Table 3. Performance indices of sine wave tracking with increased inertia.

	RMSE	MAE
DSC	0.1120	0.461
DSFTSC	0.0714	0.309
DSFTSC+FESO	0.0419	0.212

the parametric uncertainty can be reduced. Moreover, the power terms in DSFTSC also improve the accuracy. However, the backlash nonlinearity is still not well compensated. In the aspect of the DSFTSC+FESO, we can see from the "Observation" in Fig. 7 that the lumped disturbance can be observed rapidly by the FESO. Therefore, besides the advantages of the DSFTSC, the DSFTSC+FESO further reduces the periodic jumps caused by the backlash nonlinearity with the help of FESO and shows the smallest error among all the control algorithms. In addition, we can see that when a sine position command is set, the command and response of motor speed approximate to cosine waves and the motor current results in a distorted sine wave to generate the torque as shown in Fig. 7.

6.2.2 Sine wave tracking with increased inertia

The inertia is often regarded as one of the most important parameters which highly influence the performance. In order to verify the control performance in case of inertia change, the load inertia is increased from 10.7 kg·m^2 to 68.0 kg·m^2 and the experimental results are given in Fig. 8 and Table 3. We can see from Fig. 8 that the oscillations brought by backlash are exacerbated by the inertia change and the position errors of all control algorithms become larger than those in the first experiment. The motor speed and motor current depicted in Fig. 8 also show more violent oscillations. The DSC cannot adapt to the increased inertia and shows the largest position error. This is because the model parameters in DSC are given as the rated values of the first experiment. However, the load inertia of the practical servo system is increased in the second experiment, the fixed values in DSC cannot match the new system, leading to low control performance. The oscillations of DSC when crossing the backlash also turn out to be severe, since the flexibility of transmission mechanism becomes obvious with the increased inertia. Comparatively, the DSFTSC has the adaptability to inertia change by the update law and shows smaller position error and less oscillations. But the DSFTSC is also influenced by backlash. In the DSFTSC+FESO, the backlash nonlinearity is further compensated based on the disturbance observation shown in Fig. 8 and the position error turns out to be the smallest. In the proposed reaching law (29), when the switching function is away from the origin, the reaching coefficient decreases and the switching coefficient increases, which speeds up the convergence. When the switching function approaches the origin, the reaching coefficient increases and the switching coefficient decreases, which improves accuracy and reduces oscillations. The proposed switching function (28) also accelerates the error convergence. This experiment demonstrates that the proposed controller

can adapt to inertia increase and suppress the backlash nonlinearity at the same time.

6.2.3 Step setpoint tracking with torque disturbance

The torque disturbance can immediately affect the motor speed and the tracking performance or even cause system instability. In order to verify the performance in case of torque disturbance, we carry out this anti-disturbance experiment. Another motor is used to run in the current-loop mode to produce a 5 N·m torque disturbance (motor side) from 3 s to 3.4 s. The experimental results are given in Fig. 9 and Table 4, where SMAE represents the steady-state MAE and DMAE represents the disturbed MAE. We can see from Fig. 9 that the actual position is far from the set position at the initial stage, resulting in the large position tracking error and the large control input. Therefore, the motor speed increases rapidly. Due to the limitation of the speed command, the motor runs at its maximum speed for a period of time after reaching the maximum speed, and the position tracking error decreases rapidly. When the actual position approaches the set position, the tracking error and the control input become small, and the motor speed decreases. When the actual position reaches the set position, the control input is 0, and the motor stops. Compared to the other two control algorithms, the DSC takes longer rise time to reach the setpoint since the model parameters are given as the nominal values, which may be inaccurate. Comparatively, the model parameters of DSFTSC are identified online, and the parametric uncertainty can be weakened, which improves the performance. However, the DSC and DSFTSC are severely affected by the torque disturbance and show large disturbed error. In the DSFTSC+FESO, the torque disturbance can be observed rapidly by the FESO as shown in the "Observation" of Fig. 9 and the influence can be reduced based on the observation. This experiment demonstrates that the proposed controller has superior fast setpoint tracking and anti-disturbance abilities.

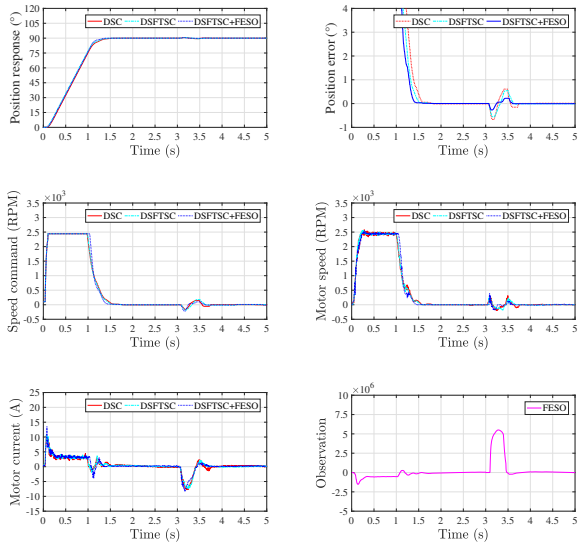

Fig. 9. Experimental results of step setpoint tracking with torque disturbance.

Table 4. Performance indices of step setpoint tracking with torque disturbance.

	Settling time	SMAE	DMAE
DSC	1.525	0.013	0.670
DSFTSC	1.398	0.008	0.555
DSFTSC+FESO	1.329	0.005	0.269

In summary, the DASTSMC+FESO can achieve fast and accurate tracking performance in both sine wave tracking and step setpoint tracking, and the FESO-based compensator can further compensate the backlash nonlinearity and torque disturbance.

7. CONCLUSION

A discrete-time modeling and control framework was proposed for electromechanical servo systems with backlash and torque disturbance. With the idea of equivalent disturbance, the nonlinear part of deadzone function and the torque disturbance were regarded as a lumped diaturbance. A FESO based on homogeneity properties was proposed to observe the lumped disturbance. Then appropriate compensation was taken to eliminate the disturbance and improve the performance of subsequent parameter estimation. Based on the compensated system, a low-order characteristic model was established. An adaptation law with projection algorithm was proposed using the tracking error and the estimation error as the excitation signal to estimate model parameters. A DSFTSC was proposed based on discrete-time model, where the improved reaching law enhanced the rapidity and weakened oscillations. The effectiveness of the proposed strategy was finally verified by experiments. The framework in this article extends the characteristic modeling to disturbed nonlinear systems and also has application prospect in other motion control systems.

CONFLICTS OF INTERESTS

The authors declared no potential conflicts of interest with respect to the research, authorship, or publication of this article.

REFERENCES

[1] T.-H. Oh, J.-S. Han, Y.-S. Kim, D.-Y. Yang, S.-H. Lee, and D.-I. Cho, "Deep RL based notch filter design method for complex industrial servo systems," *International Journal*

of Control, Automation, and Systems, vol. 18, no. 2, pp. 2983-2992, October 2020.

[2] G. Silveira, L. Mirisola, and P. Morin, "Decoupled intensity-based nonmetric visual servo control," *IEEE Transactions on Control Systems Technology*, vol. 28, no. 2, pp. 566-573, March 2020.

[3] R. Lagneau, A. Krupa, and M. Marchal, "Automatic shape control of deformable wires based on model-free visual servoing," *IEEE Robotics and Automation Letters*, vol. 5, no. 4, pp. 5252-5259, October 2020.

[4] P. C. O. Martins, A. S. De Paula, S. H. S. Carneiro, and D. A. Rade, "Hybrid control technique applied to an aero-servo-viscoelastic simplified wing model," *Aerospace Science and Technology*, vol. 122, pp. 1-17, March 2022.

[5] Z. Xu, X. Zhou, H. Wu, X. Li, and S. Li, "Motion planning of manipulators for simultaneous obstacle avoidance and target tracking: An RNN approach with guaranteed performance," *IEEE Transactions on Industrial Electronics*, vol. 69, no. 4, pp. 3887-3897, April 2022.

[6] X. Wang, B. Wang, X. Chen, and J. Yu, "Discrete-time position tracking control for multimotor driving systems via multipower terminal sliding-mode technique," *IEEE/ASME Transactions on Mechatronics*.

[7] C. Froehlich, W. Kemmetmuller, and A. Kugi, "Model-predictive control of servo-pump driven injection molding machines," *IEEE Transactions on Control Systems Technology*, vol. 28, no. 5, pp. 1665-1680, September 2020.

[8] R. C. Roman, R. E. Precup, E. L. Hedrea, S. Preitl, I. A. Zamfirache, C. A. Bojan-Dragos, and E. M. Petriu, "Iterative feedback tuning algorithm for tower crane systems," *Proc. of 8th International Conference on Information Technology and Quantitative Management*, vol. 199, pp. 157-165, 2022.

[9] H. Ucgun, I. Okten, U. Yuzgec, and M. Kesler, "Test platform and graphical user interface design for vertical take-off and landing drones," *Romanian Journal of Information Science and Technology*, vol. 25, no. 3-4, p. 350, 2022.

[10] Y. Zhao, Z. Li, K. Zhou, X. Liao, W. Guan, W. Wan, S. Yang, J. C. Cao, D. Xu, S. Barbieri, and H. Li, "Active stabilization of terahertz semiconductor dual-comb laser sources employing a phase locking technique," *Laser & Photonics Reviews*, vol. 15, no. 4, 2000498, April 2021.

[11] Q. Mo, J. Yu, C. Chen, W. Cai, S. Zhao, H. Li, and Z. Zang, "Highly efficient and ultra-broadband yellow emission of lead-free antimony halide toward white light-emitting diodes and visible light communication," *Laser & Photonics Reviews*, vol. 16, no. 10, 2100600, October 2022.

[12] W. Zhang, L. Stern, D. Carlson, D. Bopp, Z. Newman, S. Kang, J. Kitching, and S. B. Papp, "Ultranarrow linewidth photonic-atomic laser," *Laser & Photonics Reviews*, vol. 14, no. 4, 1900293, April 2020.

[13] M. Wang, H. Wang, W. Li, X. Hu, K. Sun, and Z. Zang, "Defect passivation using ultrathin PTAA layers for efficient and stable perovskite solar cells with a high fill factor and eliminated hysteresis," *Journal of Materials Chemistry A*, vol. 7, no. 46, pp. 26421-26428, December 2019.

[14] S. Chen, S. Xue, D. Zhai, and G. Tie, "Measurement of freeform optical surfaces: trade-off between accuracy and dynamic range," *Laser & Photonics Reviews*, vol. 14, no. 5, 1900365, May 2020.

[15] Z. Zuo, J. Song, W. Wang, and Z. Ding, "Adaptive backstepping control of uncertain sandwich-like nonlinear systems with deadzone nonlinearity," *IEEE Transactions on Systems, Man, and Cybernetics: Systems*, vol. 52, no. 11, pp. 7268-7278, November 2022.

[16] S. Wang and J. Na, "Parameter estimation and adaptive control for servo mechanisms with friction compensation," *IEEE Transactions on Industrial Informatics*, vol. 16, no. 6, pp. 6816-6825, November 2020.

[17] J. Wang, Y. Gao, Y. Liu, J. Liu, G. Sun, and L. Wu, "Intelligent dynamic practical-sliding-mode control for singular Markovian jump systems," *Information Sciences*, vol. 607, pp. 153-172, August 2022.

[18] H. Jin, X. Zhao, and T. Wang, "Novel load disturbance observer-based global complementary sliding mode control for a precision motion stage driven by PMLSM," *International Journal of Control, Automation, and Systems*, vol. 19, no. 11, pp. 3676-3687, November 2021.

[19] T. Zeng, X. Ren, and Y. Zhang, "Fixed-time sliding mode control and high-gain nonlinearity compensation for dual-motor driving system," *IEEE Transactions on Industrial Informatics*, vol. 16, no. 6, pp. 4090-4098, June 2020.

[20] P. Li, L. Wang, G. Zhu, and M. Zhang, "Predictive active disturbance rejection control for servo systems with communication delays via sliding mode approach," *IEEE Transactions on Industrial Electronics*, vol. 28, no. 2, pp. 12679-12688, December 2021.

[21] Y. Bai, J. Hu, and J. Yao, "Adaptive neural network output feedback robust control of electromechanical servo system with backlash compensation and disturbance rejection," *Mechatronics*, vol. 84, pp. 1-14, June 2022.

[22] W. Yao, Y. Guo, Y. Wu, and J. Guo, "Robust adaptive dynamic surface control of multi-link flexible joint manipulator with input saturation," *International Journal of Control, Automation, and Systems*, vol. 20, no. 2, pp. 577-588, February 2022.

[23] B. Wang, M. Iwasaki, and J. Yu, "Command filtered adaptive backstepping control for dual-motor servo systems with torque disturbance and uncertainties," *IEEE Transactions on Industrial Electronics*, vol. 69, no. 2, pp. 1773-1781, February 2022.

[24] Y. Zhang, J. Guo, and Z. Xiang, "Finite-time adaptive neural control for a class of nonlinear systems with asymmetric time-varying full-state constraints," *IEEE Transactions on Neural Networks and Learning Systems*.

[25] Y. Zhang, M. Chadli, and Z. Xiang, "Predefined-time adaptive fuzzy control for a class of nonlinear systems with output hysteresis," *IEEE Transactions on Fuzzy Systems*.

[26] X. Wang, B. Wang, Y. Wu, J. Guo, and Q. Chen, "Adaptive control and disturbance compensation for gear transmission servo systems with large range inertia variation," *Transactions of the Institute of Measurement and Control*, vol. 44, no. 3, pp. 700-715, February 2022.

[27] L. V. Truong, S, D, Huang, V. T. Yen, and P. V. Cuong, "Adaptive trajectory neural network tracking control for industrial robot manipulators with deadzone robust compensator," *International Journal of Control, Automation, and Systems*, vol. 18, no. 9, pp. 2423-2434, September 2020.

[28] G. Sun, J. Zhao, and Q. Chen, "Observer-based compensation control of servo systems with backlash," *Asian Journal of Control*, vol. 23, no. 1, pp. 499-512, January 2021.

[29] Z. Xu, S. Li, X. Zhou, S. Zhou, and T. Cheng, "Dynamic neural networks for motion-force control of redundant manipulators: an optimization perspective," *IEEE Transactions on Industrial Electronics*, vol. 68, no. 2, pp. 1525-1536, February 2021.

[30] B. Wang, M. Iwasaki, and J. Yu, "Finite-time command filtered backstepping control for dual-motor servo systems with LuGre friction," *IEEE Transactions on Industrial Informatics*, vol. 19, no. 5, pp. 6376-6386, May 2023.

[31] H.-W. Kim, H.-J. Kim, and J.-Y. Choi, "Multiparameter identification for SPMSMs using NLMS adaptive filters and extended sliding-mode observer," *IET Elecrric Power Applications*, vol. 14, no. 4, pp. 533-543, April 2020.

[32] J. Wang, F. Wang, G. Wang, S. Li, and Y. Li, "Generalized proportional integral observer based robust finite control set predictive current control for induction motor systems with time-varying disturbances," *IEEE Transactions on Industrial Informatics*, vol. 14, no. 9, pp. 4159-4168, September 2018.

[33] L. Zhang, J. Yang, and S. Li, "A model-based unmatched disturbance rejection control approach for speed regulation of a converter-driven DC motor using output-feedback," *IEEE/CAA Journal of Automatica Sinica*, vol. 9, no. 2, pp. 365-376, February 2022.

[34] Z. Xu, X. Yang, W. Zhang, W. Zhang, L. Zhang, and P. Liu, "Backstepping sliding mode control based on extended state observer for robotic manipulators with LuGre friction," *International Journal of Control, Automation, and Systems*, vol. 20, no. 6, pp. 2054-2066, June 2022.

[35] H. Wu, J. Hu, and Y. Xie, "Characteristic model-based all-coefficient adaptive control method and its applications," *IEEE Transactions on Systems, Man, and Cybernetics, Part C (Applications and Reviews)*, vol. 37, no. 2, pp. 213-221, March 2007.

[36] H. Wu, J. Hu, and Y. Xie, *Characteristic Model-based Intelligent Adaptive Control*, China Science and Technology Press, Beijing, China, 2009.

[37] L. Chen, X. Yu, and C. Sun, "Characteristic modeling approach for complex network systems," *IEEE Transactions on Systems, Man, and Cybernetics: Systems*, vol. 48, no. 8, pp. 1383-1388, August 2018.

[38] Z. Zuo, X. Ju, and Z. Ding, "Control of gear transmission servo systems with asymmetric deadzone nonlinearity," *IEEE Transactions on Control Systems Technology*, vol. 24, no. 4, pp. 1472-1479, July 2016.

[39] W. Perruquetti, T. Floquet, and E. Moulay, "Finite-time observers: application to secure communication," *IEEE Transactions on Automatic Control*, vol. 53, no. 1, pp. 356-360, February 2008.

[40] S. P. Bhat and D. S. Bernstein, "Geometric homogeneity with applications to finite-time stability," *Mathematics of Control, Signals and Systems*, vol. 17, no. 2, pp. 101-127, May 2005.

[41] S. P. Bhat and D. S. Bernstein, "Lyapunov analysis of finite-time differential equations," *Proceedings of 1995 American Control Conference*, pp. 1831-1832, 1995.

[42] H. Du, X. Yu, M. Z. Q. Chen, and S. Li, "Chattering-free discrete-time sliding mode control," *Automatica*, vol. 68, pp. 87-91, June 2016.

[43] E. Zhao, J. Yu, J. Liu, and Y. Ma, "Neuroadaptive dynamic surface control for induction motors stochastic system based on reduced-order observer," *ISA Transactions*, vol. 128, pp. 318-328, September 2022.

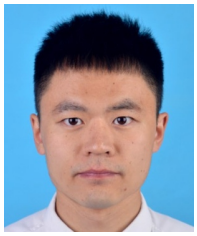

Xiang Wang received his B.S. degree in electrical engineering and automation and a Ph.D. degree in control science and engineering at Nanjing University of Science and Technology, Nanjing, China, in 2013 and 2020, respectively. He is currently a Lecturer at the School of Automation, Nanjing Institute of Technology, Nanjing, China. His research interests include servo system, system identification, and nonlinear control.

Hanzhong Liu received his M.S. degree in mechanical and electronic engineering at Nanjing University of Science and Technology, Nanjing, China, in 2004. He was a visiting scholar at Hong Kong University of Science and Technology, Hong Kong, China, in 2019. He is currently a Professor at the School of Automation, Nanjing Institute of Technology, Nanjing, China. His research interests include motion control, robotic control, fault diagnosis, and health monitoring.

Jiali Ma received his B.Sc. degree in automation and a Ph.D. degree in control science and engineering at Nanjing University of Science and Technology, Nanjing, China, in 2015 and 2020, respectively. He is currently a Professor at the School of Automation, Nanjing University of Science and Technology, Nanjing, China. His research interests include nonlinear systems, multi-agent system control, and neural network control.

Yang Gao received his B.Sc. degree in automation and a Ph.D. degree in control science and engineering at Nanjing University of Science and Technology, Nanjing, China, in 2015 and 2021, respectively. He is currently a Postdoctor at the School of Automation, Nanjing University of Science and Technology, Nanjing, China. His research interests include adaptive control, servo system, and fault tolerant control.

Yifei Wu received his Ph.D. degree in control science and engineering at Nanjing University of Science and Technology, Nanjing, China, in 2014. He is currently an Associate Professor at the School of Automation, Nanjing University of Science and Technology, Nanjing, China. His research interests include servo system and ultra high speed motor control.